Advances in Environmental and Life Sciences 2 (2022) 32-43

Contents lists available at Egyptian Knowledge Bank

Advances in Environmental and Life Sciences

journal homepage: https://aels.journals.ekb.eg

Preparation and Characterization of Eco-friendly Nanocomposite for Methylene Blue Dye Removal from Industrial Wastewater

Abbas M Abbas,[a] Adel S Orabi [a], Sayed A Eltohamy [b], Rasha A Shoman [b,*]

[a] Chemistry Department, Faculty of Science, Suez Canal University. Ismailia, 41522, Egypt.

[b] Environmental Research Department, Land, Water and Environment Institute, Agricultural Research Center(ARC), Ministry of Agriculture and Land Reclamation, 9-Cairo university street, Giza, 12112, Egypt.

Abstract

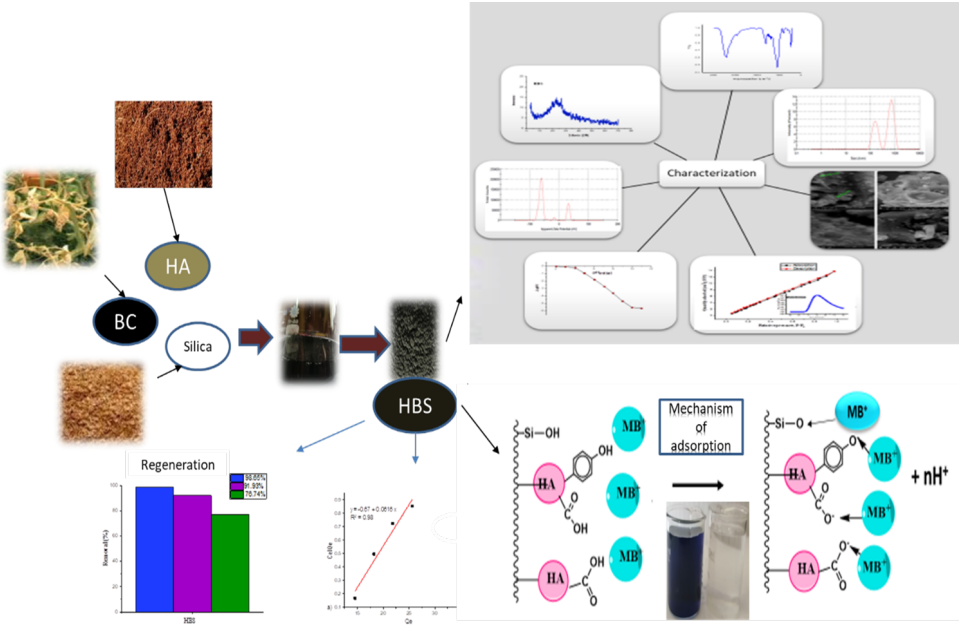

A new nanocomposite (HBS) was prepared based on humic acid, biochar, and silica using the coprecipitation method for methylene blue dye removal from industrial wastewater. The humic acid, biochar, and silica are produced from compost, tomato residual, and Rice husk feedstocks. The HBS nanocomposite was characterized by FTIR, XRD, SEM, Zeta potential, BET, and SEM-EDX. The mean surface area, average pore volume, average crystal size, and surface charge of the nanocomposite were 41.68 m^2/g, 4.20 nm of 9.95nm, and negatively charged surface with nanosized crystals, respectively. The batch experiments included the effect of dose, initial concentration, pH, connect time, temperature, and isothermal model. The optimum conditions for removing methylene blue from wastewater are 50 mg of HBS, 100 mg/L (initial concentration), pH 9, and contact time of 60 min at room temperature. The adsorption process was endothermic and fitted with the Langmuir model. The maximum adsorption capacity was 16.23 mg/g. The negative value of ΔG^o indicates the spontaneous process of adsorption. The HBS nanocomposite was successfully regenerated in three cycles for the removal of MB.

Keywords: Humic acid, Biochar, Silica, Methylene Blue, and Nanocomposite

* Corresponding author:
Emailaddress:rose5shoman@gmail.com(Rasha A. Shoman)

doi 10.21608/AELS.2022.137498.1013

Received: 13 May 2022, Revised: 6 June 2022
Accepted: 8 June 2022: Published: 8 June 2022

1. Introduction

Environmentalists are increasingly concerned about how important to keep the environment clean to ensure the survival of aquatic and terrestrial life, including humans [1]. Heavy metals and dyes are only two of many pollutants that have ruined the environment and jeopardized the general public's health [2].

The dyeing industry's effluents, which contain a high concentration of suspended organic solids, are among the most polluting to the environment [3]. In addition to harming aquatic life, untreated discharge of this colored water into receiving water bodies is also carcinogenic and mutagenic to humans. The release of these effluents concerns reasons related to toxicology and the environment [4].

The removal of suspended particulates and the lowering of chemical oxygen demand are helpful in biological treatment processes. However, removing color from wastewater has been mainly ineffectual [5]. As a result, physicochemical approaches for eliminating color from textile effluent have been studied. Each method's benefits and drawbacks have been thoroughly analyzed [6] [7]. Chemical oxygen demand (COD) can be reduced by adsorption as an effective and cost-effective means of removing many types of colorants and dyes [7].

Methylene Blue is a highly potent monoamine oxidase inhibitor (MAOI) in vitro and causes potentially fatal serotonin toxicity in humans. Gastrointestinal disturbances and urinary incontinence are the most dangerous side effects of methylene blue misused. Large doses of methylene blue can produce methemoglobinemia, chest pain, dyspnea, restlessness, apprehension, tremors, a sense of oppression, urinary tract irritation, and mild hemolysis with moderate hyperbilirubinemia, reticulosis, and slight anemia [8].

Dyes removal from wastewater can be accomplished using conventional methods, like flocculation, adsorption, ozonation, electrochemical techniques, and fungal decolorization. As a result of its established ability to remove contaminants from effluents to stable forms, adsorption is a highly effective and cost-effective method of removing dyes and other colorants [9].

Activated carbon (AC), inorganic oxides, and natural adsorbents (such as clays and clay minerals, cellulosic materials, chitin, and chitosan) have been extensively used as adsorbents [10].

The purpose of this work was to prepare ecofriendly, sustainable, good mechanical, chemical resistance, handleable, and regeneratable nanocomposite from a natural source such as humic acid, silica, and biochar for methylene blue dye removal from industrial wastewater and study the thermodynamic, kinetics, and mechanism adsorption of methylene blue (MB), on prepared nanocomposite.

2. Experimental

2.1. Materials

Methylene blue was purchased from Sigma Aldrich. HCl, NaOH, and $AgNO_3$ were purchased from Biochem. A compost sample and rice husk ash were purchased from Moshtohaor Agriculture Research Station. Tomato residual for biochar production has been collected from the agricultural area in Romana, North Sinai, and Egypt.

2.2. Characterization Techniques:

The atomic absorption spectrophotometer type AA-6800, Shimadzu, Japan, is used to determine the concentrations of metal ions. Infrared spectroscopy (FTIR) is performed using a Bruker Tensor instrument. 27 spectrophotometers (KBr disc) in the range of 400-4000 cm^{-1}. Muffle furnace Stuart Scientific (Vulcan A-550). The point zero charges (pHpzc) for the nanocomposite were determined by solid addition. In this method, 100 mg of the nanocomposites were added to a 50ml of 0.05 M KNO_3. The pH values for these solutions have been adjusted from 2 to 11 with increment 1(initial pHs'). Either 0.1 M HCl or 0.1 M NaOH solutions were used to adjust the pH values. Each flask was then vigorously agitated in a shaker bath for 48 h. each flask was shaken violently in a shaker bath. The final pHs of each suspension were determined. These values were then plotted against each other to see how much of a difference between them.

The PZC was defined as the pH at which the pH is zero. The Zetasizer Ver.7.13 (Malvern P analytical) analyzed 1mg of composite in 10 ml of water (or additives solutions) for particle size distribution and Zeta potential. The BET equation calculated the composite's specific surface area (Brunauer-Emmett-Teller). For microporous and mesoporous volumes, N_2 adsorption-desorption isotherm data from Dubinin-Radushkevich and Barrett, Joyner, and Halenda methods are used (BJH). We used SEM with an EFI S50 Inspect, the Netherlands at 30 kV, and an Energy Dispersive Spectrometer (EDS) to observe the samples for a detailed morphological analysis of the adsorbed materials (EDX, Thermofisher). Wafers were coated with silver carbon or silver lacquer and then tested on these. The pH values were measured by pH meter (KnicK pH-meter model 761 Climatic) after calibrating using buffer solutions of pH 4, 7, and 10.

X-ray powder diffraction pattern was obtained using a Rigaku Miniflex X-ray diffractometer. The Scherrer equation was used to estimate particle size from XRD data.

Crystalline size = (0.9 λ / B cosθ) (1)

Where λ, θ, and B are wavelength, Bragg angle, and the line widening are the full width at half maximum (FWHM) was achieved from the spectrum curve, measured between those points on the y-axis, which are half the maximum amplitude. Origin 8.5 was used for such calculations.

The antimicrobial activity of HBS was tested. The composite dissolved with sodium hydroxide and neutralized by dilute HCl control. Results are presented as the diameter of the inhibitory zone measured in "mm" samples (0.06 mg/disc) were analyzed using the disc diffusion method [11] against the following indicator strains: Staphylococcus aureus is referred to as "Staph" (ATCC 25923). Escherichia coli is known as "E.coli" (ATCC 25922). Candida albicans (ATCC 10231).

2.3. Solutions preparation

To prepare a stock solution of methylene blue (1000 mg/L), 0.5 g of methylene blue was weight into a 500 mL volumetric flask and then deionized until the sign. The working solution is prepared by suitable dilution with deionized until. 0.01 N $AgNO_3$ has been prepared as a standard solution for determining chloride ions by precipitation titration using potassium chromate as the indicator.

2.4. Nanocomposite preparation

Fig. (1) summarize the preparation steps of the nanocomposite. Equal weights of humic acid and silica (500 mg) were mixed and dissolved in 15mL of 0.5N NaOH; 50 mg of biochar was added after complete dissolution. The mixture was stirred for 24 hours for homogenization. The solid composite (HBS) was formed by acidifying the solution to a pH less than 2.0 using 2N HCl. The composite was collected by centrifuging for 15 minutes at 6000 rpm. The composite (HBS) was washed with deionized water to remove chloride ions.

2.5. The adsorption capacity and Isotherm

The adsorption capacity was performed using the batch mode with an adsorbent dosage of 50 mg and an adsorbate volume of 10 mL at the indicated adsorbent concentrations. Filtration of the liquid phase was completed after the equilibrium time. The initial MB concentrations ranged from 75 to 200 mg/L; the contact period ranged from 0–120 min, the pH modified from 3 to 9, and the temperature from 25 to 50 °C.

The Percentage of removal, the removal efficiency, and the adsorption capacity (q_e mg/g) at equilibrium for the removal of dye were calculated using the following equations [12]:

$$Removal\,(\%) = \frac{(C_o - C_e)}{C_o}\, x100 \quad (2)$$

$$q_e = \frac{(C_o - C_e) * V}{m} \qquad (3)$$

Where q_e is the equilibrium adsorption capacity, C_o is the initial concentration of MB, C_e (mg/L) is the equilibrium concentration, V is the sample volume (L), and m is the mass of composite (adsorbent) (g).

Three isotherm equations, Langmuir, Freundlich, and Temkin, are examined in this study [13]. The adsorption sites are comparable in the Langmuir adsorption isotherm, and

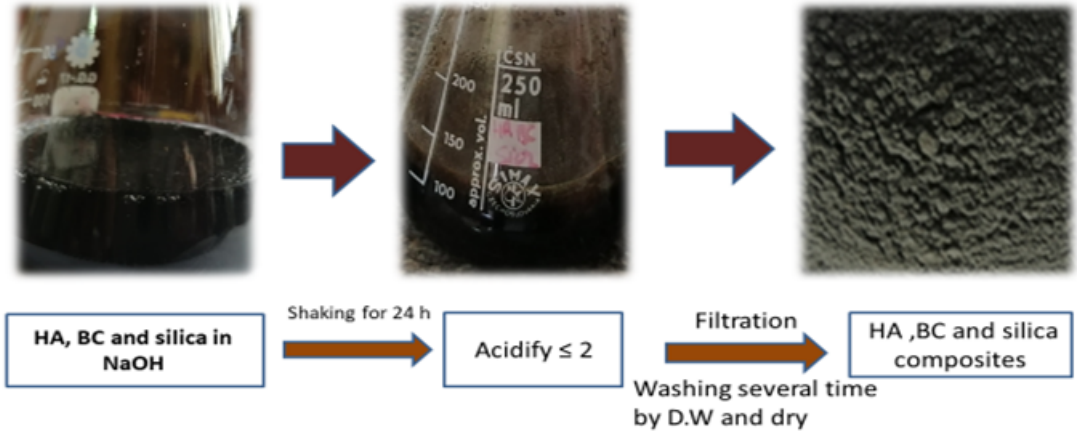

Figure 1: Schematic preparation and purification of HBS.

static adsorption sites are unaffected by whether neighboring sites are occupied. According to the Langmuir isotherm equation, the data on uptake has been analyzed [14].

$$\frac{C_e}{Q_e} = \frac{1}{Q_m} C_e + \frac{1}{Q_{mK_L}} \qquad (4)$$

C_e adsorption concentrations (mg/L), Q_e adsorbate adsorption capacities (mg/g), Q_m the maximum monolayer coverage capacity, and K_L Langmuir isotherm constant (L/mg).

An arbitrary constant separation factor R_L can be used to express the Langmuir isotherm's fundamental properties, as shown in equation 5 [14]:

$$R_L = \frac{1}{(1 + K_L C_o)} \qquad (5)$$

Adsorbate concentration (mg/L) at the highest point of adsorption is C_o. If $R_L > 1$, the isothermal shape is unfavorable; if $R_L = 1$, linear; favorable; if R_L 1, irreversible; if $R_L = 0$, the isothermal shape is unfavorable.

Using the Freundlich isotherm, one can describe heterogeneous systems empirically. Equation (below) describes this design [15]:

$$Q_e = K_f C_e^{1/n} \qquad (6)$$

This equation has the following linear form:

$$\ln Q_e = \frac{1}{n} \ln C_e + \ln K_F \qquad (7)$$

In these equations, K_F is the Freundlich constant or maximum absorption capacity, and C_e is the solution concentration equilibrium (mg/L).

If K_F measures the sorbent's adsorption capacity, it accurately indicates how well the adsorption process progresses. 1/n, the exponent, is a good indicator of the adsorption preference. 1/n < 1 implies that the adsorption is typical. If the number n is between 1 and 10, the absorption process is considered successful [16].

According to the Temkin adsorption model, the heat of adsorption for all molecules in the layer decreases linearly as coverage increases [17]. Following is the equation that describes the model:

$$Q_e = B \ln C_e + b \ln A \qquad (8)$$

Where (A) is the value of the Temkin isotherm constant, B = RT/b, which is the Temkin constant related to the heat of sorption (K J/mol) and R is the gas constant (8.314 J/mol K).

2.6. Adsorption Thermodynamics parameters

The thermodynamic equilibrium coefficients were obtained and used to study adsorption thermodynamic parameters at various temperatures and concentrations. When discussing a material's ability to adsorb, one can use thermodynamic quantities such as the Gibbs free energy change (ΔG^o) to explain the adsorption characteristics, which can be calculated by the following equation [18]:

$$\Delta G^o = -RT \ln K_d \qquad (9)$$

In which K_d denotes the equilibrium thermodynamic constant (L g^{-1}).

The adsorption enthalpy (ΔH^o) and entropy (ΔS^o) are divided by the temperature to arrive at

the Gibbs free energy (ΔG^o). The Van't Hoff plot can be used to determine ΔH^o and ΔS^o by applying this concept to the equations (9) and (10):

$$LnK_d = -\Delta H^o/RT + \Delta S^o/R \quad (10)$$

2.7. Adsorption kinetics

Adsorption kinetics must be studied thoroughly to gain insight into the course and mechanism of the processes. This study used experimental data from various contact times to test multiple pseudo-first- and second-order kinetic models. Adsorption rate constant can be calculated with a pseudo-first-order equation (Lagergren equation) [19]:

$$\log (Q_e - Q_t) = \log Q_e - \frac{K_1}{2.303} t \quad (11)$$

Here K_1 is the pseudo-first-order rate constant (min^{-1}).

It is possible to express pseudo-second-order kinetics as an integrated second-order rate law [20]:

$$\frac{t}{Q1} = \frac{1}{Qe} t + \frac{1}{K_2 Q_e^2} \quad (12)$$

K_2 is the pseudo-second-order rate constant (g mg^{-1} min^{-1}). There are two types of processes here: chemical and physical, which are included in pseudo-second-order adsorption. There are valence forces at play here, as the adsorbent and adsorbate share or exchange electrons, which could be the rate-limiting step [20].

2.8. Regeneration of nanocomposite

MB dye was desorbed by treating MB@HBS with 6 N HCl at ambient temperature and then washed with deionized water [21]. The reusability was investigated by running four consecutive cycles of adsorption−desorption. After each run, the recovery efficiency, R (%), was calculated as follows:

$$Recovery\ (\%) = \frac{C_{des}}{C_{ads}} x\, 100 \quad (13)$$

Where C_{des} and C_{ads} are the amounts of MB desorbed into the aqueous solution and the amount of MB dye adsorbed onto the composite nano-adsorbents (mg/L).

3. Results and discussion

3.1. Characterization

3.1.1. Infrared spectroscopy

The IR spectral data of Humic acid, biochar, silica, and HBS are shown in **Fig. (2)**. Broadband at 3425-3419 cm^{-1} of O-H and N–H. the broadness was caused by H-bonding, the prominent absorbance bands of humic acid. Aliphatic C–H stretching of humic acid showed at 2934–2932 cm^{-1}; Olefinic and aromatic C–C stretching causes a band at 1648–1645 cm^{-1}; COOH stretching causes a band at 1648–1645 cm^{-1}; aromatic C–C stretching content in quinone and amide causes a band at 1638–1510 cm^{-1}; a more pronounced peak at 1422-1384 cm^{-1} due to COO^- symmetric stretching, A weak band at 1384-1332 cm^{-1} due to OH deformation and C-O stretching of phenolic OH, C–H deformation of CH_2 and CH_3 groups, COO-anti-symmetric stretching, a band at 1125-1122 cm^{-1}due to aliphatic CH_2, OH or C–O groups N–H bending stretching, a peak at 1042-1029 cm^{-1} due to C–O stretching of carbohydrates, and finally a band at 601-589 cm^{-1} due to Para-di-substituted aromatic ring bend [22].

Table (S1) lists the biochar FT-IR spectra, which exhibit significant discrepancies in their infrared spectra (**Fig. 2**). On the other hand, the bands of carboxylic acids around (1638 cm^{-1}) and phenol alcohols around (3419 cm^{-1}) can also be observed. The chief absorbance bands of biochar were collected: Broadband at 3454-3419 cm^{-1}due to H-bonding of O-H and N–H groups. A strong band around 1637-1620 cm^{-1} may be assigned for C=O or C=C stretching of olefinic, aromatic, ketones (trace), quinone, and amide. A weak band at 1384cm^{-1} is caused by the deformation of phenolic OH and the stretching of the C-O ring. A band around 1125-1122 cm^{-1} was caused by the deformation of aliphatic CH_2, OH, or C–O groups. A peak at 1042-1029 cm^{-1} was caused by the stretching of the C–O ring. Finally, the deformation of the C–H ring results appeared at 616-474 cm^{-1} [23].

For FTIR of silica, the broad bands at 470 and 1100 cm^{-1}, assigned to Si–O–Si and the silicate ion, can be seen in **Fig. (2)** and listed in **Table (S1).** The 3419 cm^{-1} sorption peak in the purified silica spec-

trum indicates the presence of the hydroxyl group of Si-OH in the spectrum. [24].

HBS exhibited broadband at 3455-3416 cm^{-1} due to OH and NH groups involved in H-bonding. C=O stretching, Olefinic, Aromatic C=C stretching, C=O ketones (trace), an aromatic C=C, and the conjugated ketones quinone and amide at 1638-1509 cm^{-1}. The aliphatic C–H band, C–H deformation of the CH_2 and CH_3 groups, COO^- antisymmetric stretching, OH deformation and C=O stretching of phenolic OH, C–H deformation of CH_2 and CH_3 groups, COO^- symmetric stretching appeared at 1459-1448 cm^{-1}. A sharp peak around 1104-1000 cm^{-1} due to the terminal group of the silanol group (Si-OH), a peak at 802 cm^{-1} due to aromatic ethers, possibly polysaccharides, and Si-O of silicates, and finally, a band at 805 cm^{-1} [25].

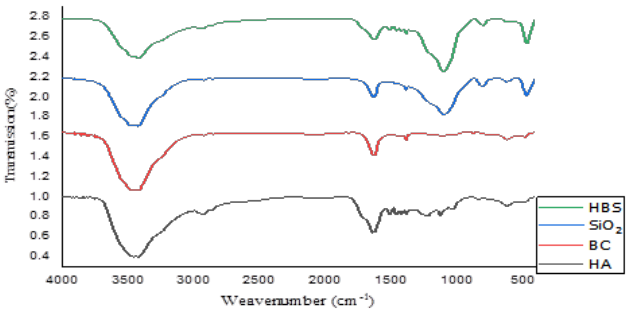

Figure 2: FT-IR spectrum of humic acid, biochar, silica and HBS.

3.1.2. *The X-ray powder diffraction (XRD pattern)*

XRD patterns for humic acid and silica showed a diffuse pattern, which indicates an amorphous phase (**Fig. (3) and Fig. (S2)**). The humic acid and nano-silica particles formed an agglomerate with a 10-30 nm diameter. The distribution of particle shapes appears to be nearly uniform. Broadening the X-ray bands of biochar allowed an estimate of the average particle size as 52.4 nm. The X-ray powder diffraction (XRD) pattern of HBS has an average crystal size of 9.95 nm using the Scherrer equation [26].

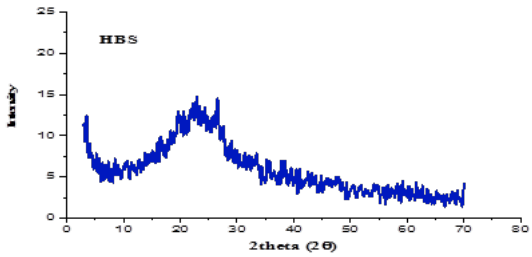

Figure 3: XRD of HBS.

3.1.3. *Particle size distribution*

Particle size distribution indicates the sizes of particles present and the proportions in the dispersion [27]. The particle size distribution of HBS was calculated in water; the data are cited in **Table 1** and shown in **Fig. (S3)**. The data showed that the composite has two sizes in the dispersant. The values are 712 nm (63.4%), 158 nm (36.6%).

3.1.4. *Zeta potential*

Zeta potential is negative for HBS, as illustrated in **Table 1** and shown in **Fig (S4)**. The value of potential for HBS is -41.5mV due to carboxylic groups and phenolic groups on surface nanocomposites. Amine groups may cause a small positive peak that appeared. This result agrees with the FTIR of the nanocomposite. For the study of the variation of the surface charge with pH values, PZC was performed as shown in **Fig (S5)**; at pH 3, the charge was equal to zero.

3.1.5. *BET Analysis*

Type III composite nanoparticle isotherm refers to an isotherm that is convex to the x-axis across its entire range and is hence reversible. Unrestrained multilayer formation can also be seen. In adsorbed molecules, lateral interactions are more powerful than those between the adsorbent and adsorbate [28], as shown in BET surface area for HBS was 41.68 m^2/g, which is the first steep area for the cross-sectional area of the N_2 molecule in the isotherm for 16.2 nm and 3.2718e+001 nm average particle radii. A saturation pressure of 1 bar results in 0.07 cm^3/g of pore volume, with an average diameter of 4.22nm and 0.07 cm^3/g of liquid volume at that pressure. Its surface area was 34.65

Table 1: Sizedistribution and Zeta potential analysis of HBS, dispersant is water,dispersant RI is 1.330 and viscosity is 0.8872cP.

Size (nm)	% intensity	St . Dev.	Z-Average (nm)	PdI	Intercept
712.0	63.4	180.5	623.8	0.540	0.872
158.4	36.6	40.28			
Mean(mV)	% Area	St. Dev.	Zeta potential (mV)	Zeta Deviation (mV)	Conductivity (mS/cm)
-62.2	75.6	6.32	-41.5	38.8	0.0129
31.7	20.8	3.78			
-16.6	2.5	2.87			

m^2/g, its pore volume 0.09 cm^3/g, and the diameter of its pores Dv (d) 1.63 nm. There was an increase in adsorption surface area of 41.68 m^2/g (due to the t-plot approach) (**Fig (S6)** and **Table (S2)**).

3.1.6. SEM-EDX analysis

Fig. (4) showed the SEM of HBS, which appeared as an irregular surface. SEM was used to indicate the nanocomposite's surface roughness and porosity.

Fig. (5) shows the SEM-EDX analysis results of HBS before and after MB adsorption C, O, and Si is the primary components of humic acid, biochar, and silica. Adsorption EDX confirms the presence of MB in the materials.

3.2. The adsorption processes

The batch method was used for the adsorption process, as shown in **Fig. (S7-S11)**. Removal of MB dye increased by HBS has removal efficiency of MB dye was from 96.62% when the dose was 30 mg to 99.95% for 300 mg, and adsorption capacity decreased from 32.21 mg/g to 3.33 mg/g. Adsorption tests on HBS were carried out in various pH solutions to investigate the impact of pH on the material's adsorption capacities. MB uptake by HBS depends on the pH of the aqueous solution. The adsorption capacity of methylene blue sorption decreases from 19.64 to 15.88 mg/g when the initial pH of the solution decreases from 9 to 3. Proportion removal of MB lowered from 35.22 mg/g to 14.51 for HBS when concentration increased from 75 to 200 mg/L. The adsorption is almost constant at whatever dye concentration if all of the sites are occupied. The results suggest the formation of a monolayer on the composite surface that has been prepared. The adsorption reached equilibrium within 5min (16.07 mg/g) for the initial concentrations after it became nearly constant. The percent of MB was removed gradually with time increases and reached its maximum level after 60 min (19.46 mg/g). The adsorption of MB dye (19.77-19.65 mg/g) on HBS was achieved at (25- 55^{o}C).

3.3. Adsorption isotherm

The equilibrium data for the adsorption process are usually termed adsorption isotherms. It is necessary to know them to compare the effectiveness of various adsorbent substances under different operational conditions and to layout and improve an adsorption system. Usually, adsorption is shaped by the classical adsorption isotherms [29]. Three isotherms models were used. Langmuir, Freundlich, and Temkin isotherms values of various constants of the three models were calculated and represented in **Table 2**.

Langmuir-Friendlich-Temkin-like linearized forms for removing MB from water using HBS as an adsorbent are presented in **Fig. (S12).** It was observed that. The experimental data fitted well with all the isotherm models.

In Langmuir's study, the correlation coefficients (R^2) give values of 0.98 for MB. Langmuir coefficient b is an indicator of the stability of the compound produced between MB and HBS under specific experimental conditions. In this study, the small K_L values -0.09 L.mg^{-1} were obtained, which indicates a strong binding of pollutants to the HBS

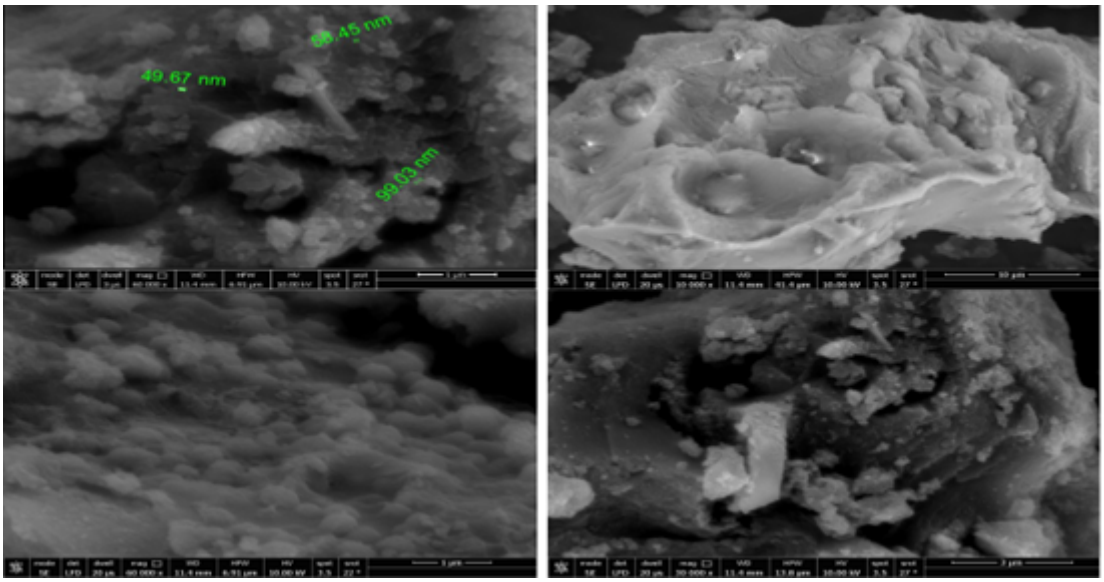

Figure 4: SEM of HBS.

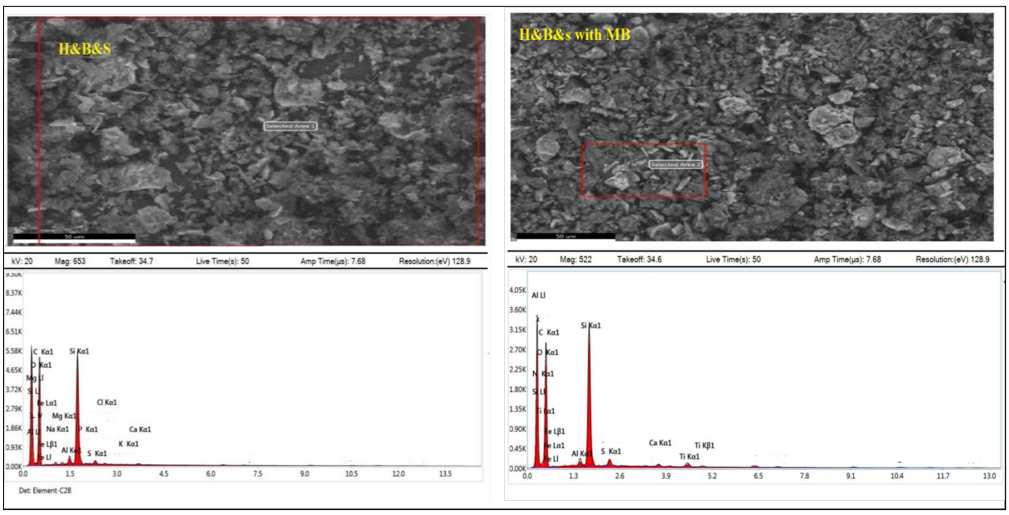

Figure 5: EDX of nanocomposite without addition and with additionof MB.

surface. In this study, the R_L value was less than 1, which suggested that the adsorption of MB on HBS is favorable and fitted the Langmuir isotherm model. In this study, the R_L value for MB was found to be -0.08, which is less than 1.

In the Freundlich study, the n value for MB adsorption was 3.13. Because 1/n values smaller than 1 suggest concave isotherms and sorbates with lower free energy, favorable adsorption can be seen in the isotherm. The correlation coefficients (R^2) give a value of 0.896, which is the highest value compared to the Temkin model. It was observed that the Freundlich isotherm provides a good fit model than the Temkin isotherm model. Thus, the adsorption of MB onto HBS follows a multilayer adsorption process.

In the Temkin study, it was observed that the heat of sorption is equal to 324.25 $Jmol^{-1}$ for MB.

Table 3 summarises the q_{max} values of several adsorbents reported in the literature. HBS composite exhibits good MB dye adsorption capacity when compared to prior studies, according to the findings of this investigation. HBS's employment in removing MB dye is highly promising due to its widespread availability, low cost, and intriguing adsorption potential.

Table 2: Parameters and correlation coefficient ofLangmuir, Freundlich and Temkinisotherm model for adsorption of MB dye onto HBS.

Langmuir isotherm model parameters	Qm (mg/g)	16.23
	K_L= (L/mg)	-0.09
	R_L	-0.08
	R^2	0.98
Freundlich isotherm model parameters	1/n	0.32
	n	3.13
	K_F (mg/g (L/mg)1/n)	10
	R^2	0.896
Temkin isotherm model parameters	A (L/g)	6.10
	b (J/mol)	324.25
	B	7.00
	R^2	0.83

Table 3: Monolayeradsorption capacities (q_{max} in mg/g) in the literature foradsorption of methylene blue on various adsorbents.

Adsorbent	pH	Temperature (^{o}C)	q_{max} (mg/g)	References
HBS	7	25	16.23	This study
Acid- activated milled pyrophyllite	7	20	4.2	[30]
Natural zeolite	7	25	5.5	[31]
Modified ZSM-5 Zeolite	4	25	23	[32]
Cold plasma modified kaolin	8	30	23	[33]
Modified play grorskite	6.5	20	33	[34]
Wheat shells			21.5	[35]
perlite	11	30	0.7	[36]

3.4. Adsorption Thermodynamics

ΔH° and ΔS° were calculated using a linear plot of lnK_d versus 1/T and its slope and y-intercept. ΔH° was 6.38 kJ mole^{-1}, and ΔS° was only 0.03 kJ mole^{-1}K^{-1}, according to the data presented in **Fig. (S13)**. Enthalpy ΔH° of HBS with the addition of MB was 6.38 kJmol^{-1} and 0.03 KJ/mol^{-1}, respectively, as depicted in **Fig. (S13)** and illustrated in **Table 4**.

The following equation (13) was used to calculate ΔG^o at various temperatures. [37]:

$\Delta G^o = \Delta H^o + T\Delta S^o$ (13)

Adsorption occurs spontaneously when ΔG^o is negative at these temperatures. The positive ΔH° implies that this adsorption is endothermic, stating that this adsorption is accelerated at low temperatures, indicating that a temperature rise could increase the number of dye-binding sites on the adsorbent surface. Adsorbate molecules spread more quickly throughout the adsorbent particles' exterior limit layer and internal pores as the solution's viscosity decrease due to the increasing temperature [38]. As the adsorbent undergoes structural changes, a modestly positive value of ΔS^o indicates increased entropy in the solid/liquid interface [39].

3.5. Adsorption kinetics

Table 5 and **Fig. (S14)** indicate R^2 values above 0.99997 for various situations in the pseudo-second-order model, which is better than the pseudo-first-order model's linearity. According to the results of the pseudo-second-order model, qe_{cal} data matched up well with the experimental

Table 4: Thethermodynamic parameters of MB adsorption on HBS.

The values of the thermodynamic of MB dye					
ΔH^o	ΔS^o	ΔG^o (kJ/mol)			
(kJ/mol)	(kJ/mol.K)	298	313	318	323
6.38	0.03	-24.15	-29.83	-29.35	-25.06

data. Therefore, the pseudo-second-order model is a good fit for HBS nanocomposite MB adsorption kinetics.

Table 5: Parametersof pesudofirst-order and pseudosecond-order for adsorption of MB onto HBS.

pesudofirst-order			pseudosecond-order		
Q_e cal	K_1	R^2	Q_e cal	K_2	R^2
1.60	0.07	0.82	20.10	0.06	0.99997

3.6. Adsorption mechanism

Langmuir isotherm and pseudo-second-order model best describe the adsorption of MB on HBS, which are most correlated with the experimental results over the whole range investigated. It is assumed that the surface of the HBS, which contains reactive –OH groups like carboxylic and phenolic groups binding MB, is homogenous. The operating adsorption mechanism is chemisorption onto a homogenous surface, which can be very well matched to the adsorption of MB. Ion exchange is the most widely accepted mechanism, as shown in **Fig. (6).**

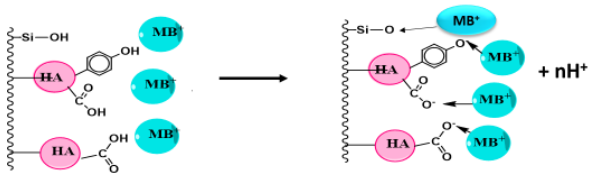

Figure 6: Mechanism of MB dye adsorption on HBSnanocomposite.

3.7. Regeneration of HBS

For regeneration investigation and stability of nanocomposite, several cycles were checked. In the present work,

At 25 °C, the extraction of MB dye from HBS was completed. The adsorbed material was recorded through filtration; it was then washed with parts of 6N HCl, deionized water, and dried for two days in a temperature-controlled environment. HBS that had been regenerated had its adsorption performance compared to that of fresh HBS under the same test conditions. MB dye solution of 100 mg/L and pH 7 was prepared by adding 50 mg of regenerated adsorbent. Comparison of regenerate's absorption capacity with an unregenerate's (**Fig. (S15)**) Adsorption capacity was good. The material was stable, so it could be used repeatedly without losing any potent properties.

It can be concluded that the synthesized HBS can act as a highly renewable and stable adsorbent for practical application and can satisfy the increasing need for the purification of water resources.

The Langmuir isotherm adsorption capacity parameter q_{max} is frequently used to assess adsorbent performance.

4. Conclusion

The research clearly shows that HBS composites are an effective adsorbent to remove MB dye economically from aqueous solutions. The nanocomposite HBS characterized by have negatively charged surface with nanosized crystals. The surface area was found from BET studies at 41.68 m^2/g, and it has carboxylic, phenolic, and silanol groups. The maximal capacities (q_{max}) of methylene blue sorption decrease from 19.64 to 15.88 mg/g when the initial pH of the solution decreases from 9 to 3. In the adsorption studies, While the Langmuir model correctly predicted equilibrium adsorption results with a maximum adsorption capacity of 16.23 mg/g, the pseudo-second-order model better represented the kinetic

uptake features. The adsorption process appears to be endothermic and spontaneous based on the measured thermodynamic characteristics. HBS was found to be an effective MB adsorbent, according to the data.

References

[1] S. Rodríguez-Zaragoza, Ecology of Free-Living Amoebae 20 (2008) 225–241. doi:doi.org/10.3109/10408419409114556.

[2] M. E. Ossman, M. Abdelfattah, in: and others (Ed.), International Conference on Agricultural, Chemical, Biological and Environmental Sciences, 2018, pp. 60–65. [link].
URL https://uruae.org/siteadmin/upload/4576AE06182011.pdf

[3] S. Mani, P. Chowdhary, R. N. Bharagava, Textile Wastewater Dyes: Toxicity Profile and Treatment Approaches, Emerging and Eco-Friendly Approaches for Waste Management (2019) 219–244doi:doi.org/10.1007/978-981-10-8669-4_11.

[4] S. Madhav, Water Pollutants: Sources and Impact on the Environment and Human Health, Sensors in Water Pollutants Monitoring: Role of Material. Advanced Functional Materials and Sensors. (2020) 43–62doi:doi.org/10.1007/978-981-15-0671-0_4.

[5] F. El-Gohary, A. Tawfik, Decolorization and COD reduction of disperse and reactive dyes wastewater using chemical-coagulation followed by sequential batch reactor (SBR) process, Desalination 249 (3) (2009) 1159–1164. doi:doi.org/10.1016/j.desal.2009.05.010.

[6] N. Kannan, M. M. Sundaram, Kinetics and mechanism of removal of methylene blue by adsorption on various carbons-a comparative study, Dye. Pigment 51 (1) (2001) 25–40.

[7] K. H. Gonawala, M. J, M. I, Removal of color from different dye wastewater by using ferric oxide as an adsorbent, J. E. R. Appl, (2014).

[8] X. Jin, M. Jiang, X. Shan, Z. Pei, Z. C. .-J. Of, C. Interface (2008). [link].
URL https://www.sciencedirect.com/science/article/pii/S0021979708010904

[9] K. Mahmoudi, K. Hosni, N. Hamdi, E. Srasra, Kinetics and equilibrium studies on removal of methylene blue and methyl orange by adsorption onto activated carbon prepared from date pits-A comparative study, Korean J. Chem. Eng 32 (2) (2015) 274–283.

[10] V. Katheresan, J. Kansedo, S. Y. Lau, Efficiency of various recent wastewater dye removal methods: A review, J. Environ. Chem. Eng 6 (4) (2018) 4676–4697. doi:doi.org/10.1016/j.jece.2018.06.060.

[11] C. Avşar, H. Özler, I. Berber, S. C, .-I. F. Research, Phenolic composition, antimicrobial and antioxidant activity of Castanea sativa Mill. pollen grains from Black Sea region of Turkey (2016).

[12] P. Wang, M. Cao, C. Wang, Y. Ao, J. Hou, J. Qian, Kinetics and thermodynamics of adsorption of methylene blue by a magnetic graphene-carbon nanotube composite, Appl. Surf. Sci 290 (2014) 116–124.

[13] A. Bonilla-Petriciolet, D. Mendoza-Castillo, Adsorption Processes for Water Treatment and Purification, 2017. doi:DOI 10.1007/978-3-319-58136-1.

[14] H. Swenson, N. P. Stadie, Langmuir's Theory of Adsorption: A Centennial Review, Langmuir 35 (16) (2019) 5409–5426. doi:doi.org/10.1021/acs.langmuir.9b00154.

[15] R. Saadi, Z. Saadi, R. Fazaeli, N. E. Fard, Monolayer and multilayer adsorption isotherm models for sorption from aqueous media, Korean Journal of Chemical Engineering 32 (2015) 787–799. doi:DOI: 10.1007/s11814-015-0053-7.

[16] A. Nimibofa, E. A. Newton, W. Donbebe, Modelling and Interpretation of Adsorption Isotherms, Journal of Chemistry 2017 (2017) 1–11. doi:doi.org/10.1155/2017/3039817.

[17] P. S. Kumar, S. Ramalingam, C. . Senthamarai, M. Niranjanaa, Adsorption of dye from aqueous solution by cashew nut shell: studies on equilibrium isotherm, kinetics and thermodynamics of interactions, Desalination 261 (1-2) (2010) 52–60. doi:doi.org/10.1016/j.desal.2010.05.032.

[18] X. Hu, J. songWang, Y. guoLiu, Adsorption of chromium (VI) by ethylenediamine-modified cross-linked magnetic chitosan resin: isotherms, kinetics and thermodynamics, Adsorption of chromium (VI) by ethylenediamine-modified cross-linked magnetic chitosan resin: isotherms, kinetics and thermodynamics 185 (1) (2011) 306–314. doi:doi.org/10.1016/j.jhazmat.2010.09.034.

[19] D. G. Strawn, A. M. Scheidegger, D. L. Sparks, Kinetics and mechanisms of Pb(II) sorption and desorption at the aluminum oxide - Water interface, Environ. Sci. Technol 32 (17) (1998) 2596–2601.

[20] L. Seifi, Kinetic study of BTEX removal using granulated surfactant-modified natural zeolites nanoparticles, Water. Air. Soil Pollut 219 (1-4) (2011) 443–457.

[21] M. Adel, M. A. Ahmed, A. A. Mohamed, A facile and rapid removal of cationic dyes using hierarchically porous reduced graphene oxide decorated with manganese ferrite, FlatChem 26 (2021) 100233–100233.

[22] K. Sugahara, A. Inoko, Composition analysis of humus and characterization of humic acid obtained from city refuse compost, Soil Sci. Plant Nutr 27 (2) (1981) 213–224.

[23] J. T. Yu, A. M. Dehkhoda, N. Ellis, Development of biochar-based catalyst for transesterification of canola oil, Energy and Fuels 25 (1) (2011) 337–344.

[24] E. Rafiee, S. Shahebrahimi, Nano Silica with High Surface Area from Rice Husk as a Support for 12-Tungstophosphoric Acid: An Efficient Nano Catalyst in Some Organic Reactions, Chinese J. Catal 33 (7-8) (2012) 60420–60428.

[25] A. F. Hassan, A. M. Abdelghny, H. Elhadidy, A. M. Youssef, Synthesis and characterization of high surface area nanosilica from rice husk ash by surfactant-free sol-gel method, J. Sol-Gel Sci. Technol 69 (3) (2014) 465–472.

[26] F. T. L. Muniz, M. A. R. Miranda, C. M. Santos, J. M. Sasaki, The Scherrer equation and the dynamical theory of X-ray diffraction, Acta Crystallogr. Sect. A Found. Adv 72 (3) (2016) 385–390.

[27] M. Gill, S. P. Armes, D. Fairhurst, S. N. Emmett, G. Idzorek, T. Pigottt, Particle Size Distributions of Polyaniline-Silica Colloidal Composites, Langmuir 8 (9) (1992) 2178–2182.

[28] M. Kruk, M. Jaroniec, Gas adsorption characterization of ordered organic-inorganic nanocomposite materials, Chem. Mater 13 (10) (2001) 3169–3183.

[29] T. H. Tran, Adsorption isotherms and kinetic modeling of methylene blue dye onto a carbonaceous hydrochar adsorbent derived from coffee husk waste, Sci. Total Environ 725 (2020) 138325–138325.

[30] J. Sheng, Y. Xie, Y. Zhou, Adsorption of methylene blue from aqueous solution on pyrophyllite, Applied Clay Science 46 (4) (2009) 422–424. doi:doi.org/10.1016/j.clay.2009.10.006.

[31] R. Han, J. Zhang, P. Han, Y. Wang, et al., Study of equilibrium, kinetic and thermodynamic parameters about methylene blue adsorption onto natural zeolite, Chemical Engineering Journal 145 (3) (2009) 496–504. doi:doi.org/10.1016/j.cej.2008.05.003.
URL https://www.sciencedirect.com/science/article/pii/S1385894708002568

[32] X. Jin, Adsorption of methylene blue and orange II onto unmodified and surfactant-modified zeolite, Adsorption of methylene blue and orange II onto unmodified and surfactant-modified zeolite 328 (2) (2008) 243–247. doi:doi.org/10.1016/j.jcis.2008.08.066.

[33] Ö. Yavuz, C. Saka, Surface modification with cold plasma application on kaolin and its effects on the adsorption of methylene blue, Applied Clay Science 85 (1) (2013) 96–102. doi:DOI: 10.1016/j.clay.2013.09.011.

[34] J. Zhang, D. Cai, et al., Adsorption of methylene blue from aqueous solution onto multiporous palygorskite modified by ion beam bombardment: Effect of contact time, temperature, pH and, Adsorption of methylene blue from aqueous solution onto multiporous palygorskite modified by ion beam bombardment: Effect of contact time, temperature, pH and 83-84 (2013) 137–143. doi:doi.org/10.1016/j.clay.2013.08.033.

[35] Y. Bulut, H. Aydin, A kinetics and thermodynamics study of methylene blue adsorption on wheat shells, Desalination 194 (1-3) (2006) 259–267. doi:doi.org/10.1016/j.desal.2005.10.032.

[36] B. A, C. E, Batch kinetic study of sorption of methylene blue by perlite, Journal and undefined (2005).

[37] Y. Miyah, A. Lahrichi, M. Idrissi, A. Khalil, F. Zerrouq, Adsorption of methylene blue dye from aqueous solutions onto walnut shells powder: Equilibrium and kinetic studies, Surfaces and Interfaces 11 (2018) 74–81.

[38] J. P. Silva, S. Sousa, J. Rodrigues, H, et al., Adsorption of acid orange 7 dye in aqueous solutions by spent brewery grains, Separation and Purification Technology 40 (3) (2004) 309–315. doi:doi.org/10.1016/j.seppur.2004.03.010.

[39] A. Malik, A. Khan, N. Anwar, M. Naeem, A comparative study of the adsorption of congo red dye on rice husk, rice husk char and chemically modified rice husk char from aqueous media, Bull. Chem. Soc. Ethiop 34 (1) (2020) 41–54.